An Accurate Frequency Tracking Method Based on Short Current Detection for Inductive Power Transfer System

Xin Dai, *Member, IEEE*, and Yue Sun

***Abstract*—Frequency drifting is a common problem in an inductive power transfer (IPT) system. Conventional autonomous oscillation method for maintaining soft switching is challenged due to the drawbacks of feedback delay and disturbance, resonant failure, and requirements of additional start-up circuit. A novel frequency tracking method based on short current detection is proposed for IPT applications. In addition, an instantaneous short current detection method utilizing cheap comparator is proposed. Furthermore, a fast and accurate tracking method is proposed to calculate the frequency mismatch and make a correction. The method can realize accurate frequency correction in several oscillation periods. Furthermore, the method is simple and economic for hardware implementation. Finally, the results of the experiment and comparison results verified the frequency tracking method.**

***Index Terms*—Electromagnetic coupling, frequency control, inductive power transfer (IPT).**

I. Introduction

INDUCTIVE power transfer (IPT) technology realizes efficient energy transfer across large air gap from power supply to electrical equipment. With its rapid development, more and more applications have been emerging in recent years such as mobile phone, electrical vehicle material handling, and biomedical implants [1]–[9].

For a typical IPT system, resonant tanks are very commonly used to produce low-distortion sinusoidal oscillation and increase the system reactive capability. However, the inherent parameters of the resonant tanks may dynamically drift away from the designed parameters due to load variation and mutual coefficient change [10], [11]. It is because the mutual coupling between the primary and secondary sides will produce dynamical reflection impedance in the primary resonant tank and cause its inherent frequency drifting. In order to realize soft switching, the topology switching signal must keep up with the inherent frequency variation. It should be noted here that the inherent frequency refers to the inherent soft switching frequency of the primary inverter, which transforms dc input to high-frequency ac output. Typical frequency tracking method is a passive tracking method, which completes topology switching by detecting the zero crossing points of resonant variables [12]–[15]. This method is efficient to produce a self-sustained oscillation. However, it normally requires start-up control to produce initial oscillation, and the oscillation may fail in the low-quality-factor condition [16]–[18]. Most important of all, this method cannot realize accurate frequency tracking. There inevitably exists a short-time lag in the topology switching due to the time delay and disturbance on gate driver and detection circuit in the feedback loop. The switching time lag will result in resonant waveform distortion and augment of switching loss. In particular, according to the first wireless power standard "Qi" [19], [20], the oscillation frequency in commercial IPT product should be set in the frequency range from 110 to 205 kHz. In the high-frequency range, the system becomes more complex and sensitive because many parasite parameters will affect system performance. A tiny time delay or disturbance in the feedback path may cause the system performance to fall drastically. However, due to the inherently passive running property, it is impossible to eliminate the switching time lag and disturbance so that the frequency tracking error will always exist.

Compared with the passive tracking method, an active tracking method which completes topology switching by external switching signal is seen to be a good alternate to solve these problems. However, it is greatly relied on the tracking accuracy and speed. Since the inherent frequency is determined by an implicit high-order differential equation set, it is difficult to obtain its accurate value [21]–[23]. Furthermore, even if the inherent frequency can be calculated, the time consuming will be unaffordable for real-time tracking. Therefore, instead of the complex calculation, a simple and real-time tracking method with unknown inherent frequency is needed.

In the IPT system, its well known that the short current is adverse which should be avoided. The short current occurs when resonant tank is shorted by the switching network. It is caused by mismatch between the driving frequency and the inherent soft switching frequency of the resonant tank. A large mismatch can produce dangerous high current which may cause the switching devices to fail. It has been found that the short current occurs almost instantaneously while the mismatch appears. Therefore, it can be utilized as a fast and accurate ruler to measure the frequency error.

Manuscript received October 14, 2012; revised January 29, 2013; accepted March 13, 2013. Date of publication April 5, 2013; date of current version August 9, 2013. This work was supported by the research fund of the International Science and Technology Cooperation Plan of Chongqing under CSTC, 2011GGHZA40001. The plan is provided by the Chongqing Science and Technology Commission, Chongqing, China.

The authors are with the College of Automation, Chongqing University, Chongqing 400030, China (e-mail: toybear@vip.sina.com; syue06@cqu.edu.cn).

Color versions of one or more of the figures in this paper are available online at http://ieeexplore.ieee.org.

Digital Object Identifier 10.1109/TIE.2013.2257149

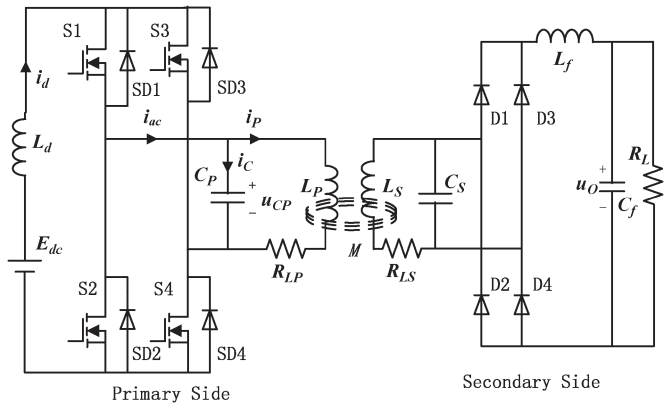

Fig. 1. Parallel-resonant-type IPT system.

This paper proposes a novel active frequency tracking method based on the detection of the short current. As the frequency drift may be higher or lower than the inherent frequency, the principles of the short current for the higher and lower case are analyzed, respectively. An instantaneous short current detection method utilizing normal comparators and field-programmable gate array (FPGA) chip is proposed. On the basis, this paper proposes a simple frequency tracking strategy based on mismatch calculation. Furthermore, a tracking error correction method is proposed as well. Finally, experimental results verified the detection and tracking control method.

II. Principles of Short Current

In terms of structures of resonant network at primary side, there are normally two types. One is parallel resonant, and the other is series resonant. The short current typically appears in parallel resonant structure. A typical parallel-resonant-type ICPT system is shown in Fig. 1.

As can be shown, the inductively coupled power transfer (ICPT) system can be divided by primary and secondary sides. At the primary side, the dc input $E_{\rm dc}$ and filter compose a quasi-current source. In addition, the switching network consists of two switch pairs (S1, S4) and (S2, S3) and their inherent inverse parallel diodes (SD1–SD4). The two switch pairs operate complementarily at the forced switching frequency, transform dc current input to high-frequency square-wave current, and inject it into the resonant network, which is composed of resonant inductor L_P, capacitor C_P, and equivalent series resistance (ESR) resistance R_{LP}. The resonant network converts the square-wave current to sinusoidal current for primary coil to produce alternating magnetic field. At the secondary side, the secondary coil will pick up energy from the magnetic field and produce resonance in the parallel resonant network composed of resonant inductor L_S and capacitor C_S. With the rectifier and filter network (L_f, C_f), ac energy is transformed to dc output to the load (R_L).

While the forced switching frequency is approaching the inherent soft switching frequency of the primary resonant network, the switching points will be close to the zero crossing points of the resonant voltage $u_{\rm CP}$ which can produce zero-voltage-switching conditions. Under the ideal conditions, there is no short current occurrence. However, due to the load and coupled coefficient parameters variation, the reflection impedance from the secondary side to the primary side will alter the parameters of primary resonant network and result in its inherent frequency drifting. The mismatch between switching frequency and inherent frequency will cause the occurrence of the short current.

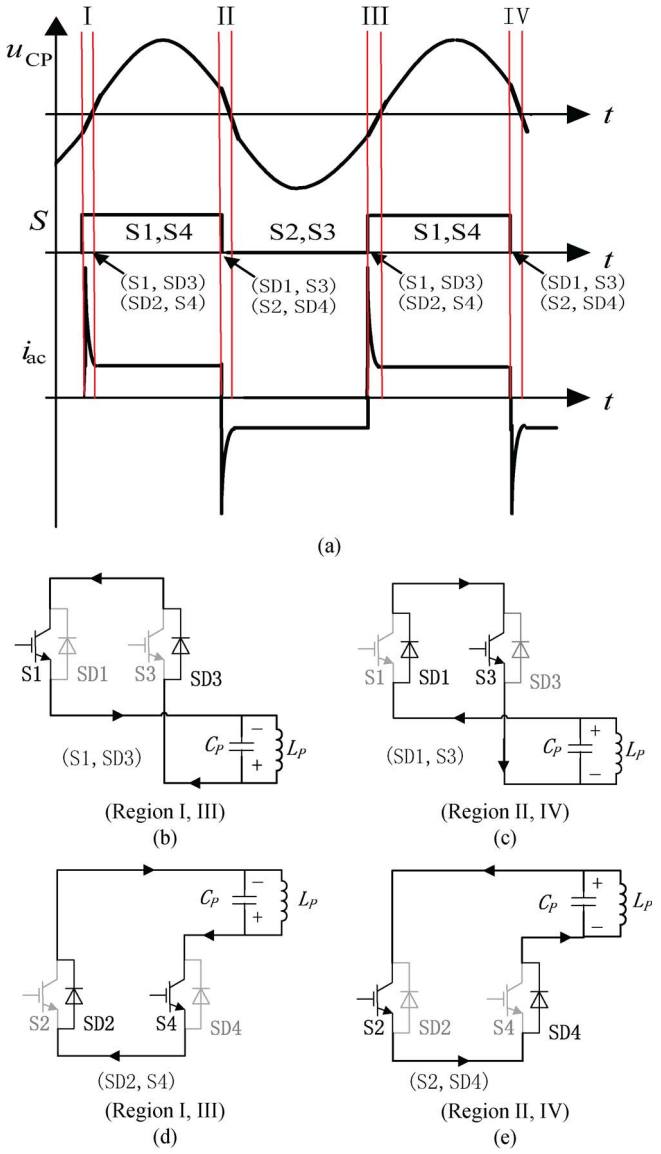

Fig. 2. Switching frequency higher case. (a) Operating waveforms when short current occurs. (b) (Regions I and III) Upper short current loop. (c) (Regions II and IV) Upper short current loop. (d) (Regions I and III) Lower short current loop. (e) (Regions II and IV) Lower short current loop.

In system running, when the switching frequency drifts away from the inherent frequency, there are two possible cases. One is higher, and the other is lower than the inherent frequency. The two cases are quite different in nature and should be analyzed, respectively.

A. Higher Case

The higher case can be illustrated in Fig. 2.

As it can be seen from (a), the waveforms from up to down are resonant capacitor voltage $u_{\rm CP}$, switching signal S, and

the input current $i_{\rm ac}$ of the resonant tank, respectively. For the switching frequency is higher than the inherent frequency, the switching instants will appear before the zero switching points of $u_{\rm CP}$. In addition, the mismatches will produce four short current regions (Region I–IV). In each region, the short current has different path and can be illustrated from (b) to (e), respectively. In Regions I and III, the switch pair (S1, S4) turns on and the switch pair (S2, S3) turns off. However, as the resonant voltage $u_{\rm CP}$ is below zero, two short current loops will form in the inverter bridge. The one shown in (b) is the upper short current loop including S1 and SD3. The other shown in (d) is the lower loop include SD2 and S4. In Regions II and IV, the switch pair (S1,S4) turn on and (S2, S3) turn off. However, the resonant voltage $u_{\rm CP}$ is above zero. Similarly, there are two short current loops. The one shown in (c) is the upper one including SD1 and S3, and the other shown in (e) is the lower one including S2 and SD4. As the total resistance in the short current path is approaching zero, the short current can be very large and result in the sharp peak of input current $I_{\rm ac}$ shown in (a).

B. Lower Case

When the switching frequency is lower than inherent frequency, the short current will appear as well. However, it is different from the higher case in nature. The lower case can be illustrated in Fig. 3.

As it can be seen from (a), since the switching frequency is lower than the inherent frequency, the switching instants will lag behind the zero crossing points of $u_{\rm CP}$. Furthermore, the mismatches will produce four short current regions (Regions I–IV). In Regions I and III, when the resonant voltage $u_{\rm CP}$ crossing the zero, the switching pair (S2, S3) still maintains ON STATE because the switching signal is lagged behind. Two short current loops will form in the upper and lower bridges, respectively. The one including SD1 and S3 is shown in (b), and the other including S2 and SD4 is shown in (d). In Regions II and IV, the switch pair (S1, S4) will maintain ON STATE. Similarly, the upper short current loop including S1 and SD3 is shown in (c), and the lower one including SD2 and S4 is shown in (e). However, it should be noted that the short current is driven by resonant inductor L_P instead of capacitor C_P as the resonant voltage is clamped to zero. Therefore, the short current peak of input current $i_{\rm ac}$ shown in (a) is much lower than that of the higher case. In addition, in higher case, the short current appears at the front end of the switching signal, while in the lower case, it appears at the back end.

III. Short Current Analysis

Since the principles of the short current are quite different in the higher and lower cases, the short current analysis should be given, respectively.

A. Higher Case

According to the analysis of the Section III, the equivalent circuit of the short current loop can be shown in Fig. 4.

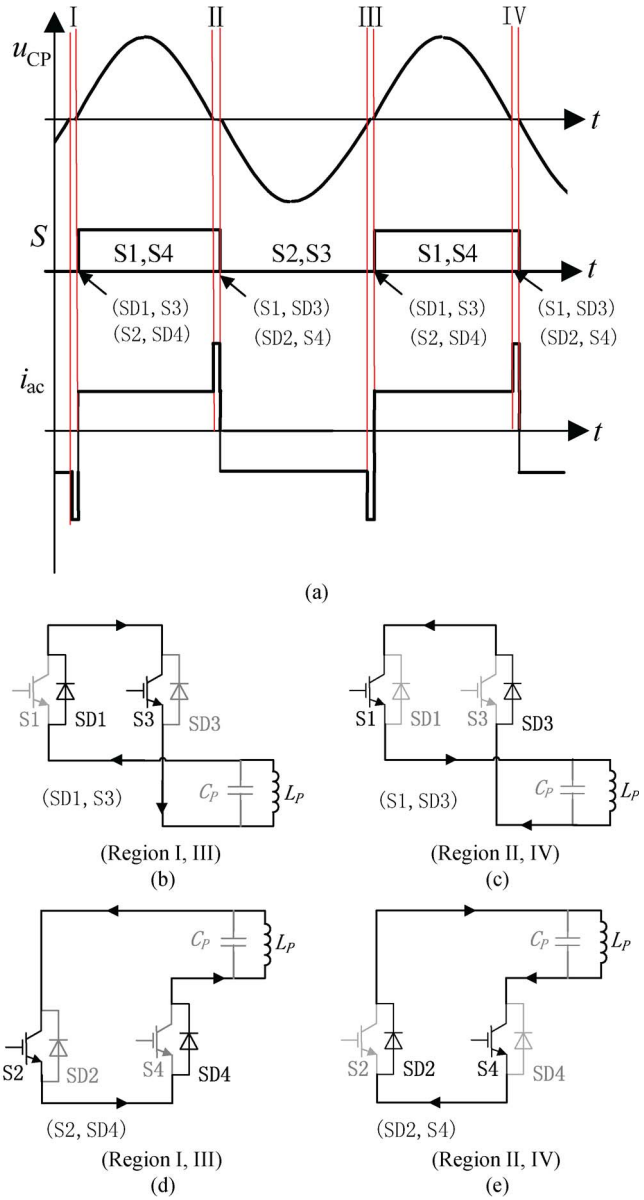

Fig. 3. Switching frequency lower case. (a) Operating waveforms when short current occurs. (b) (Regions I and III) Upper short current loop. (c) (Regions II and IV) Upper short current loop. (d) (Regions I and III) Lower short current loop. (e) (Regions II and IV) Lower short current loop.

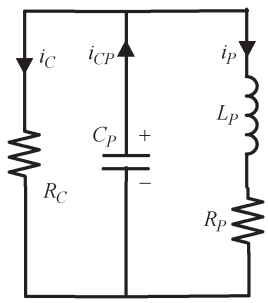

Fig. 4. Equivalent circuit of short current loop.

As can be seen, the short current is i_C, and resistance R_C is the sum of conducting resistances of switch devices and diodes on the short current loop. Moreover, the resistance R_P

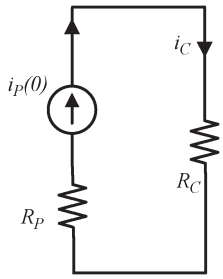

Fig. 5. Equivalent circuit of short current loop.

is the sum of ESR resistance R_{LP} and reflecting resistance from secondary side. In addition, the differential equations of the equivalent circuit can be shown as

$$\begin{cases} \frac{du_{\rm CP}}{dt} = -\frac{1}{C_P R_C}\left(u_{\rm CP} + R_C i_p\right) \\ \frac{di_P}{dt} = \frac{1}{L_p}\left(u_{\rm CP} - R_P i_p\right). \end{cases} \tag{1}$$

Because the duration time of the short current is very short, the current i_P in the inductor L_P cannot mutate at the interval. Therefore, equation $di_p/dt = 0$ can be got. Furthermore, the instantaneous resonant voltage at the time of the short current occurrence can be defined as u_{C0}. In addition, the solution of the short current can be obtained

$$i_c(t) = \frac{e^{-\frac{(R_C+R_P)t}{C_P R_C R_P}} u_{C0}}{R_C}. \tag{2}$$

The maximum short current appears at the time of short current occurrence $(t = 0)$, and it can be obtained by

$$i_{C_{(\max)}} = \frac{u_{C0}}{R_C}. \tag{3}$$

Normally, the R_C is less than 0.2 Ω. Hence, a small resonant voltage can produce a dangerous high short current which can damage the switch devices.

A threshold $I_{\rm TH}$ for the short current is defined, when the short current falls below the threshold and it can be seen as zero. In this paper, the threshold $I_{\rm TH}$ is set at 0.2 A. On the basis, the duration time T_C of the short current can be defined as the time interval from its occurrence to the moment falling below $I_{\rm TH}$. Solving the equation $i_C(T_C) = I_{\rm TH}$, the instant resonant voltage u_{C0} at the point of the short current occurrence can be obtained by

$$u_{C0} = 0.2 R_C e^{-} - \frac{(R_C + R_P)T_C}{C_P R_C R_P}. \tag{4}$$

B. Lower Case

In the lower case, the resonant voltage is clamped to zero and cannot drive the short current. The short current is actually the freewheeling current of the resonant inductor L_P. The equivalent circuit of the short current loop can be shown in Fig. 5.

In the short-time interval of the short current, the resonant current i_P can be seen as a constant, which equals the instant current $i_P(0)$ when the short current occurs. Therefore, the short current can be simply expressed as

$$i_C(t) = i_P(0). \tag{5}$$

It will be a constant in the short interval. In addition, it is obvious that the peak of the short current in the lower case is much lower than that in the higher case. Therefore, it is relatively safe when frequency is running below the inherent frequency.

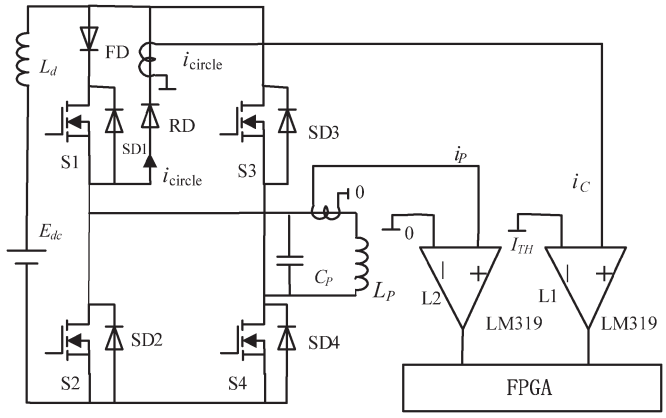

Fig. 6. Short current detection circuit.

IV. Frequency Tracking Control

The frequency tracking control is to make the switching frequency accurately and rapidly keep up with the inherent frequency variation of the resonant tank.

A. Short Current Detection

The first step of tracking is to detect the frequency mismatch. As analyzed in Section III, once the mismatch appears, the short current will occur instantly. Therefore, the short current can be utilized as the mismatch variable.

However, as the duration time of the short current is normally less than 1 μs, it is quite difficult for normal analog to digital chip to detect it. In this paper, a short current detection circuit using normal comparator chip LM319 is designed. It can be shown in Fig. 6.

As can be seen, a comparator L1 is used to detect the duration time T_C of the short current. As analyzed in Section III, two identical short currents will form in the upper and lower bridges simultaneously in no matter the higher or the lower case. Moreover, in the upper bridge, the two short current loops should include (SD1, S3) and (S1, SD3) in no matter the higher or the lower case. It can be seen that the short current in any diode of SD1–SD4 will be identical. In order to simplify the detection circuit, only SD1 is selected to detect the short current. However, as the inherent diode SD1 is normally embedded in switch device, it is difficult to detect the current on it. Therefore, an inverse parallel diode recovery diode (RD) with low conduction resistance is added to replace it. In addition, a block diode is put in series with the switch S1 to invalidate the diode SD1. Furthermore, with a current

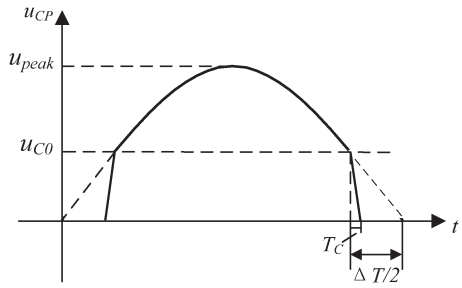

Fig. 7. Frequency mismatch calculation method for the higher case.

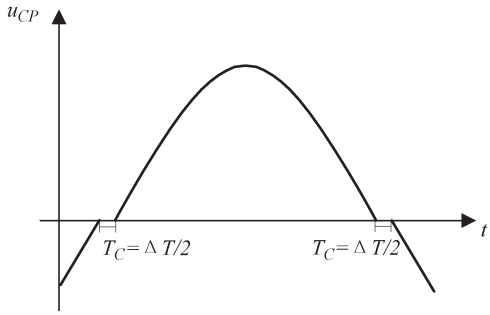

Fig. 8. Frequency mismatch calculation method for the lower case.

transformer, the short current on RD can be detected. The short current signal will be compared with the threshold reference $I_{\rm TH}$ (defined in Section III) to produce pulse signal of the short current for a FPGA chip to measure its duration time T_C.

B. Determining the Mismatch Direction

The second step of tracking is to determine whether the frequency is higher or lower than the inherent frequency. As can be seen from Figs. 2 and 3, the short current on SD1 will select different occurrence regions for the higher or lower case. For higher case, the short current will select Regions II and IV for occurrence, and for the lower case, the short current will select Regions I and III. Furthermore, it can be easily found that the Regions (I, III) and Regions (II, IV) are corresponding to the positive and negative zero crossing intervals of resonant voltage $u_{\rm CP}$, respectively. It is well known that there will be 90° phase deviation between the resonant voltage $u_{\rm CP}$ and resonant current i_P. In other words, the positive and negative zero crossing points of $u_{\rm CP}$ will be corresponding to positive max and negative max values of i_P, respectively. Therefore, a comparator L2 is used for detecting the direction of i_P in the short current interval to determine if the frequency is higher or lower than the inherent frequency.

C. Mismatching Calculation and Correction

The third step of tracking is to calculate the deviation between the switching frequency and the inherent frequency. The tracking method should be different according to the higher and lower cases. For the higher case, the frequency mismatching calculation method can be illustrated in Fig. 7.

As can be seen, with measured short current time T_C, the instant value u_{C0} of resonant voltage $u_{\rm CP}$ can be calculated by (4). In addition, the period difference can be calculated by

$$\Delta T = \frac{\arcsin\left(u_{c0}/u_{\rm peak}\right)}{\pi f_C} \tag{6}$$

where f_C is the switching frequency before the short current occurrence. In addition, $u_{\rm peak}$ can be calculated by

$$u_{\rm peak} = \frac{\pi E_{\rm dc}}{2}. \tag{7}$$

As the $u_{C0}/u_{\rm peak}$ is below one, the arc sine function can be easily calculated by lookup table to reduce the tracking time.

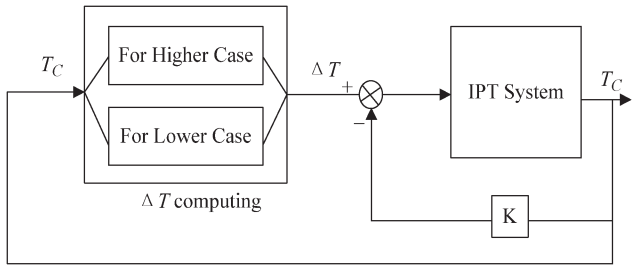

Fig. 9. Frequency tracking system structure.

For the lower case, the frequency mismatching calculation method can be illustrated in Fig. 8.

As analyzed in Section III, for the lower case, the short current will maintain constant until the switching signal is coming. Therefore, the duration time of the short current should equal half of the period deviation. Thus, the deviation can be given by

$$\Delta T = 2\,T_C. \tag{8}$$

In order to improve the accuracy of frequency tracking, a proportional feedback is designed in the system to correct the error brought by parameter drifting and measurement disturbance. The whole tracking system structure can be shown in Fig. 9.

As can be seen, only a few calculation steps are needed for frequency tracking. It is easy to embed all the calculation into an FPGA chip.

V. Experimental Study

A practical experimental IPT system has been built to verify the proposed tracking method which utilizes an FPGA chip as the tracking controller. The experimental system structure can be shown in Fig. 10.

As can be seen, in the experimental system, the detection module is set up according to Fig. 6. Only the current on inverse parallel diode RD of S1 is selected for the short current detection. The main tracking control unit (FPGA) undertakes the tasks of frequency tracking (shown in Fig. 9) and gate driving pulse generation. The feedback coefficient K for error correction is set at 0.4. The system parameters are listed in Table I.

The load change test is selected to show the tracking performance. A load bidirectional switching test from heavy

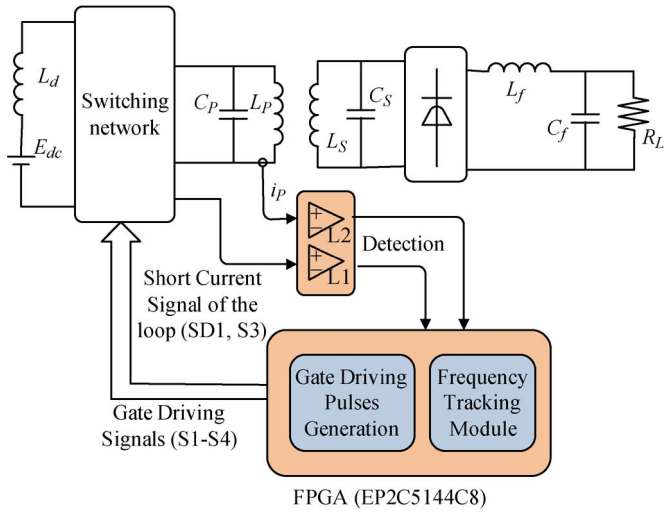

Fig. 10. Experimental system structure.

TABLE I
PARAMETER TABLE

Parameters	Values
DC input E_{dc}	30 V
Resonant inductor L_P	61.5 μH
Resonant capacitor C_P	0.47 μF
Resonant inductor L_S	152.5 μH
Resonant capacitor C_S	0.22 μF
Mutual M	31 μH

condition (corresponding to $R1 = 50\ \Omega$) to light condition (corresponding to $R2 = 200\ \Omega$) was carried out.

Fig. 11 shows the load change from the light condition $R2$ to the heavy condition $R1$; the waveforms from up to down are the short current in the loop (SD1, S3), the short current in the loop (S1, SD3), and the resonant current i_P at the primary side, respectively. The measurement method of the short current was the same as that in Fig. 6. A current transformer was used to transform the short current signal to corresponding voltage signal. The transformation ratio of current transformer is 1:1. The short current signal in the loop (SD1, S3) was utilized for frequency tracking. In addition, the short current in the loop (S1, SD3) was measured in the same way, but it was just for the purpose of comparison. There was about 30-μs adjusting time before the short current was eliminated. With the tracking control, the switching frequency was adjusted from 34.5 to 31.6 kHz. In this interval, the short current peak in the loop (SD1, S3) was 2.5 A, and the peak in the loop (S1, SD3) was 4 A. The peak value of loop (S1, SD3) was higher than the peak of loop (SD1, S3) because the loop resistance in (S1, SD3) was slightly lower than the resistance in (SD1, S3).

Fig. 12 shows the load change from heavy condition $R1$ to light condition $R2$; the waveforms are similarly defined as Fig. 11. There was about 90-μs adjusting time before the short current was eliminated. The switching frequency was adjusted from 31.6 to 34.5 kHz. In this interval, the short current peak in the loop (SD1, S3) was 2.5 A, and the peak in the loop (S1, SD3) was 3 A. In the test, it took more adjusting time than

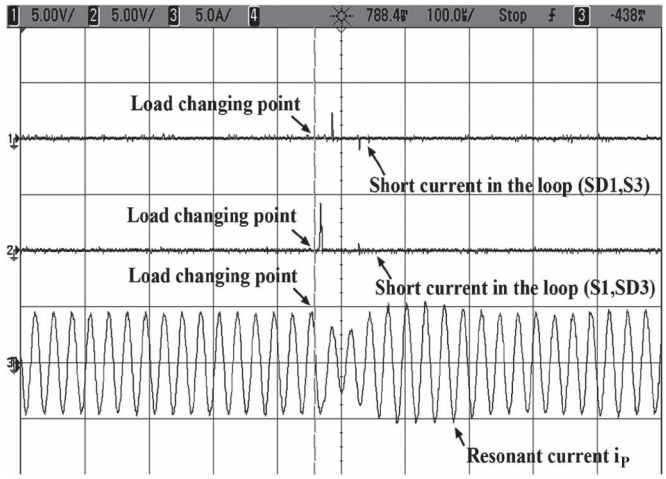

Fig. 11. Experimental waveforms of load change from $R2$ to $R1$ (from light to heavy load conditions).

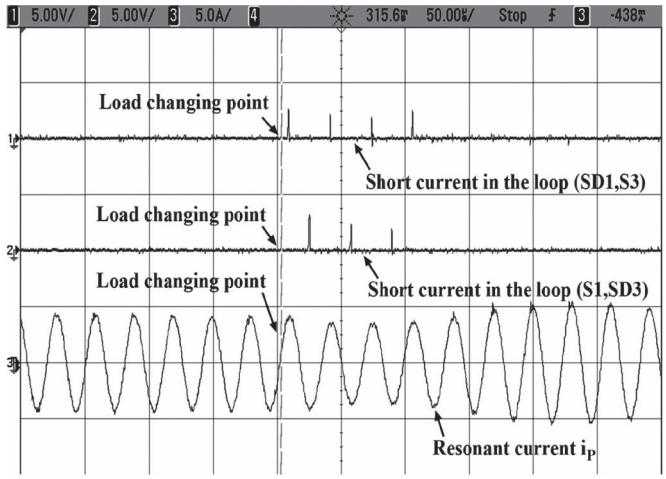

Fig. 12. Experimental waveforms of load change from $R1$ to $R2$ (from heavy to light load conditions).

that of the load changing from the light to heavy conditions. It is because load changing from heavy to light conditions will produce stronger oscillation in the resonant tank which may bring some disturbance in the feedback correction loop. However, it is relatively safe in the adjusting process due to system running under the lower case.

Fig. 13 shows the start process under the frequency tracking, and Fig. 14 shows its zoomed waveform. The system starts with the heavy load $R1$. The initial driving frequency was set at 30 kHz. It took about 350 μs to eliminate the short current. In the steady state, the running frequency was kept at 31.6 kHz. In this interval, the short current peak in the loop (SD1, S3) was 1.25A, and the peak in the loop (S1, SD3) was 1.3 A.

Fig. 15 shows the comparison between the calculated inherent frequencies and the experimental tracking frequencies with load variation. The inherent frequencies were calculated according to the iteration numerical computing method given in [23].

As can be seen, the red line denotes the calculated inherent frequencies, and the blue line denotes the experimental results. They are in good agreement. In addition, in the whole load

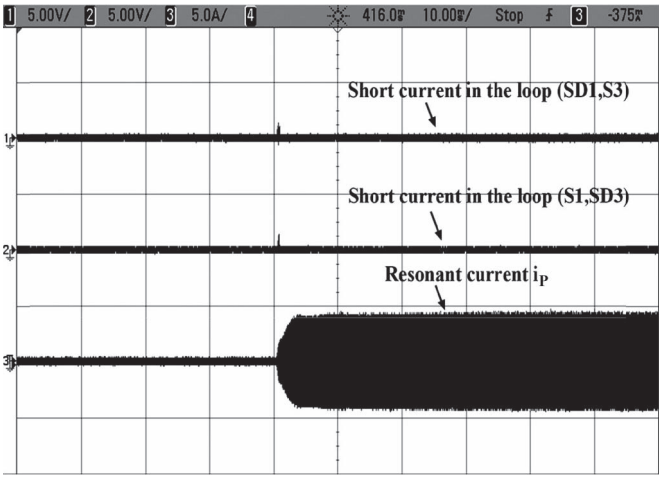

Fig. 13. Experimental waveforms of the system start process.

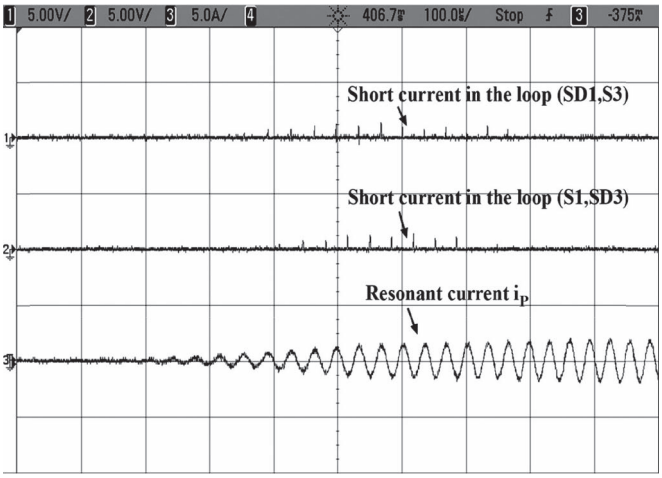

Fig. 14. Experimental waveforms of the zoomed system start process.

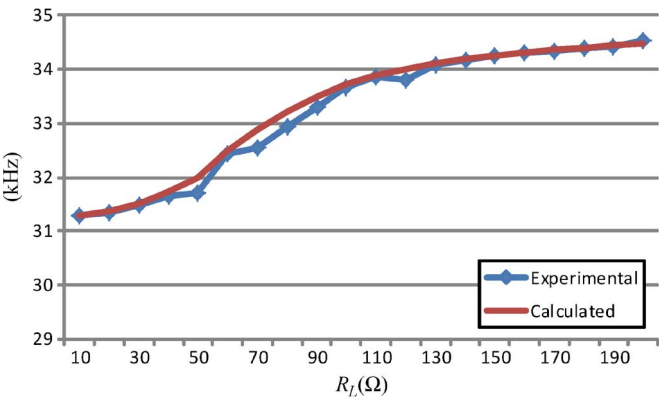

Fig. 15. Experimental and calculated results comparison.

variation range (from 10 to 200 Ω), the short current peak in the steady state was always controlled below 0.2 A. It proves that the method has an accurate frequency tracking performance.

VI. Discussion

As mentioned in Section II, there are normally two resonant types at the primary side. One is parallel resonant type which

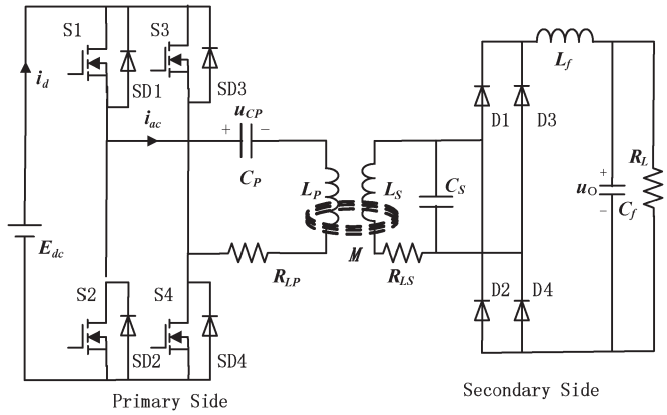

Fig. 16 Series-resonant-type IPT system.

is given and analyzed earlier. The other is series resonant type, as can be seen from Fig. 16. For the series resonant type, when frequency mismatch appears, it will not produce large short current in the upper or lower bridge as the parallel resonant type because the capacitor C_P will not be shorted. However, the short-circuit paths are the same with the parallel type. Therefore, the frequency tracking method based on short current detection can be utilized as well.

The proposed frequency tracking method based on short current detection is an accurate and instantaneous method which only allows few times of short circuit. It is affordable for low-power application. However, for high-power application, even if there is only one short current shock, the switching device may be damaged. Under this condition, the active tracking method should be utilized combining with classic passive tracking method. The passive tracking method based on zero voltage or zero current detection can be taken for a rough frequency tracking to guarantee the strength of short current in relatively safe region. In addition, the proposed active tracking method can be taken to realize accurate frequency correction.

VII. Conclusion

In this paper, a novel accurate frequency tracking method based on short current detection has been proposed for an IPT system. An instantaneous short current detection method utilizing cheap comparator is proposed. Furthermore, a fast and accurate method is proposed to calculate the frequency mismatch and make a correction. Compared with the conventional autonomous oscillation method, this method is an active one which can overcome the common problems such as feedback delay, resonant failure, and additional start-up circuit. Furthermore, the tracking strategy is simple and economic for hardware implementation. It is particularly useful for realizing soft switching in high-frequency IPT applications.

References

[1] M. Drader, "Shared coil for inductive charging and hearing-aid-compliance requirements in mobile phones," European Patent 2 450 840 A1, May 9, 2012.

[2] M. Budhia, J. T. Boys, G. A. Covic, and H. Chang-Yu, "Development of a single-sided flux magnetic coupler for electric vehicle IPT charging systems," *IEEE Trans. Ind. Electron.*, vol. 60, no. 1, pp. 318–328, Jan. 2013.

[3] S. Hasanzadeh, S. Vaez-Zadeh, and A. H. Isfahani, "Optimization of a contactless power transfer system for electric vehicles," *IEEE Trans. Veh. Technol.*, vol. 61, no. 8, pp. 3566–3573, Oct. 2012.
[4] Y. L. Ho, D. M. Budgett, and A. P. Hu, "Minimizing power loss in air-cored coils for TET heart pump systems," *IEEE J. Emerg. Sel. Topic Circuits Syst.*, vol. 1, no. 3, pp. 412–419, Sep. 2011.
[5] B. Wang, A. P. Hu, and D. Budgett, "Power flow control based solely on slow feedback loop for heart pump applications," *IEEE Trans. Biomed. Circuits Syst.*, vol. 6, no. 3, pp. 279–286, Jun. 2012.
[6] A. K. RamRakhyani, S. Mirabbasi, and M. Chiao, "Design and optimization of resonance-based efficient wireless power delivery systems for biomedical implants," *IEEE Trans. Biomed. Circuits Syst.*, vol. 5, no. 1, pp. 48–63, Feb. 2011.
[7] M. L. G. Kissin, J. T. Boys, and G. A. Covic, "Interphase mutual inductance in polyphase inductive power transfer systems," *IEEE Trans. Ind. Electron.*, vol. 56, no. 7, pp. 2393–2400, Jul. 2009.
[8] W. X. Zhong, L. Xun, and S. Y. R. Hui, "A novel single-layer winding array and receiver coil structure for contactless battery charging systems with free-positioning and localized charging features," *IEEE Trans. Ind. Electron.*, vol. 58, no. 9, pp. 4136–4144, Sep. 2011.
[9] S. L. Ho, W. Junhua, W. N. Fu, and S. Mingui, "A comparative study between novel witricity and traditional inductive magnetic coupling in wireless charging," *IEEE Trans. Magn.*, vol. 47, no. 5, pp. 1522–1525, May 2011.
[10] J. U. W. Hsu, A. P. Hu, and A. Swain, "Fuzzy logic-based directional full-range tuning control of wireless power pickups," *IET Power Electron.*, vol. 5, no. 6, pp. 773–781, Jul. 2012.
[11] J. U. W. Hsu, A. P. Hu, and A. Swain, "A wireless power pickup based on directional tuning control of magnetic amplifier," *IEEE Trans. Ind. Electron.*, vol. 56, no. 7, pp. 2771–2781, Jul. 2009.
[12] B. Sharp and H. Wu, "Asymmetrical voltage-cancellation control for LCL resonant converters in inductive power transfer systems," in *Proc. IEEE Appl. Power Electron. Conf. Expo.*, Orlando, FL, USA, Feb. 5–9, 2012, pp. 661–666.
[13] W. Yanzhen, A. P. Hu, D. Budgett, S. C. Malpas, and T. Dissanayake, "Efficient power-transfer capability analysis of the TET system using the equivalent small parameter method," *IEEE Trans. Biomed. Circuits Syst.*, vol. 5, no. 3, pp. 272–282, Jun. 2011.
[14] T. D. Dissanayake, A. P. Hu, S. Malpas, L. Bennet, A. Taberner, L. Booth, and D. Budgett, "Experimental study of a TET system for implantable biomedical devices," *IEEE Trans. Biomed. Circuits Syst.*, vol. 3, no. 6, pp. 370–378, Dec. 2009.
[15] S. Ping, A. P. Hu, S. Malpas, and D. Budgett, "A frequency control method for regulating wireless power to implantable devices," *IEEE Trans. Biomed. Circuits Syst.*, vol. 2, no. 1, pp. 22–29, Mar. 2008.
[16] A. P. Hu, G. A. Covic, and J. T. Boys, "Direct ZVS start-up of a current-fed resonant inverter," *IEEE Trans. Power Electron.*, vol. 21, no. 3, pp. 809–812, May 2006.
[17] J. T. Boys, C. I. Chen, and G. A. Covic, "Controlling inrush currents in inductively coupled power systems," in *Proc. Int. Power Eng. Conf.*, Singapore, 2005, pp. 1046–1051.
[18] J. T. Boys, A. P. Hu, and G. A. Covic, "Critical Q analysis of a current-fed resonant converter for ICPT applications," *Electron. Lett.*, vol. 36, no. 17, pp. 1440–1442, Aug. 2000.
[19] E. Waffenschmidt, "Wireless power for mobile devices," in *Proc. IEEE Int. Telecommun. Energy Conf.*, Amsterdam, The Netherlands, 2011, pp. 1–9.
[20] D. V. Wageningen and T. Staring, "The Qi wireless power standard," in *Proc. Power Electron. Motion Control Conf.*, Ohrid, Macedonia, Sep. 6–8, 2010, pp. S15-25–S15-32.
[21] C. S. Tang, Y. Sun, Y. G. Su, S. K. Nguang, and A. P. Hu, "Determining multiple steady-state ZCS operating points of a switch-mode contactless power transfer system," *IEEE Trans. Power Electron.*, vol. 24, no. 2, pp. 416–425, Feb. 2009.
[22] X. Dai and X. Y. Huang, "Study on dynamic accurate modelling and nonlinear phenomena of a push-pull soft switched converter," in *Proc. IEEE Conf. Ind. Electron. Appl.*, Singapore, May 24–26, 2006, pp. 1–4.
[23] A. P. Hu, "Selected resonant converters for IPT power supplies," Ph.D.dissertation, Dept. Elect. Comput. Eng., Auckland Univ., Auckland, New Zealand, 2001.

Xin Dai (M'10) received the B.E. degree in industrial automation from Yuzhou University, Chongqing, China, in 2000 and the Ph.D. degree in control theory and control engineering from the School of Automation, Chongqing University, Chongqing, in 2006.

In 2012, he was a Visiting Scholar with The University of Auckland, Auckland, New Zealand. He is currently a Professor with the School of Automation, Chongqing University. His current research interests include inductive power transfer technology and nonlinear dynamic behavior analysis of power electronics.

Yue Sun received the B.E. degree in electrical engineering, the M.E. degree in industry automation, and the Ph.D. degree in mechanical electrical integrated manufacturing from Chongqing University, Chongqing, China, in 1982, 1988, and 1995, respectively.

In 1997, he was a Senior Visiting Scholar with the University of Valenciennes, Valenciennes, France. He is currently a Professor with the School of Automation, Chongqing University. His current research interests include automatic control, wireless power transfer, and power electronics applications.